Pergamon

Acta Astronautica Vol. 38, Nos 4–8, pp. 395–403, 1996

0094-5765/96 $15.00 + 0.00

PII: S0094-5765(96)00052-5

AUTONOMOUS SATELLITE NAVIGATION VIA KALMAN FILTERING OF MAGNETOMETER DATA

Matthias Wiegand

Center of Applied Space Technology and Microgravity, ZARM
University of Bremen, Germany
Institute of Space Technology and Nuclear Reactor Technology, IfRR
Technical University of Braunschweig, Germany

Abstract

An autonomous orbit determination system for low earth orbiting spacecrafts is developed, simulation tested and examined using actual spacecraft data of the BREM-SAT mission. An extended Kalman-type filter is used to deduce a minimum error estimate of the spacecraft ephemeris by utilizing the knowledge of system and measurement dynamics, assumed statistics of system noises and measurement errors, and initial condition information. The presented algorithm is based on the laws of orbital mechanics and the measurement of geomagnetic field magnitude. Since low earth orbits are fully observable from a sufficient number of measurements of the strength of the Earth's magnetic field the determination scheme is independent of spacecraft attitude. In most cases the accuracy is sufficient for low earth orbiting satellites and moreover it can be used as a backup system to provide redundancy. Especially for small satellites the system is highly recommended because no additional hardware is required besides a magnetometer and computation time on the on-board computer.

I. Introduction

Several approaches in autonomous navigation have been published in the last decade. The proposed systems differ in the required technical resources and the predicted accuracy [12]. The objective of this work has been to develop an inexpensive navigation method for small satellite applications, which allows a fully autonomous orbit determination. Psiaki et al. [3, 10, 11] introduced the idea of using geomagnetic field measurements to derive spacecraft position information. This concept only requires a magnetometer and an on-board computer, both of which are commonly incorporated into various satellite designs. The orbit estimation algorithm presented in this paper only based on the observation of the magnitude of the geomagnetic field vector. The independence of the spacecraft attitude is the advantage of this formulation. Section II deals with the observability of low Earth's orbits from geomagnetic field strength measurements.

The on-board magnetometer is used to measure the local geomagnetic field, which depends upon the orbital position of the satellite. Comparisons of the measurements with the International Geomagnetic Field Model (IGRF) provide navigation information. Multiple measurements of the field strength are filtered using an extended Kalman-type filter which account for the geomagnetic field comparisons and the laws of orbital mechanics. The algorithm uses a nonlinear model of the orbital dynamics to propagate the satellite state, the position and velocity of the spacecraft (S/C), and the error covariance of the propagation. After a sufficient number of measurements, the filter converges to the best estimate of the satellite state. Section III describes the used Kalman-type filter as well as the system model and the observability model.

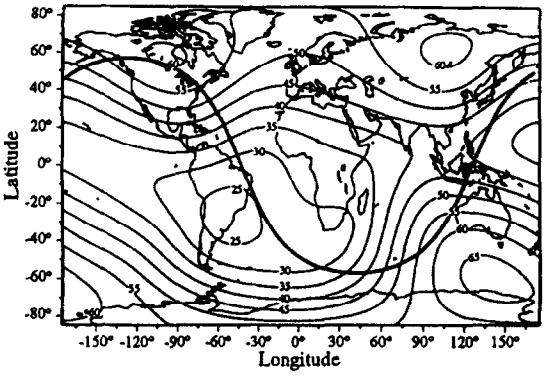

Figure 1: Total Magnetic Field Intensity in nT, epoch 1994, altitude 350 km, 10th-order IGRF model

Besides simulated data of various kinds of low Earth's orbits actual spacecraft data of the BREM-SAT mission have been used to verify this novel navigation method under very realistic conditions. The tests involve filtering of magnetometer data followed by comparison of estimated position with position derived from ground-based tracking. Section IV and V present the performance results.

II. Orbit Observability

The Earth's magnetic field vector is a function of the position regarding to the center of Earth, which means position information are included. Even if a dipole model is assumed no Keplerian orbit is identical with the contour of a constant field magnitude or remains on it for several orbits. After a certain number of measurements every low Earth's orbit is fully observable from the geomagnetic magnitude. The Kalman-type filter or state estimation methods in general uses the partial derivates of the observables with respect to the solved-for parameters to correct an a priori estimate of these parameters. Thus, higher inclinations make the orbit more observable because of larger partial derivatives. Figure 1 shows the ground-track of an orbit with 57 degree inclination. The Earth's magnetic field magnitude varies strongly over one revolution in opposite to a lower inclined orbit. For that reason equatorial orbits are rather disadvantageous but the tilt of the Earth's magnetic pole with respect to the North Pole and higher order terms of the geomagnetic field increases the observability. However, simulation testing will show the filter performance in depence on the shape of orbit.

III. Filter design

Fully observability of the orbit from measurements is necessary but only sufficient to update navigation variables in a deterministic manner, that means spacecraft position will be changed to agree with the results of a geomagnetic field measurement. If measurements are ambiguous and random measurement errors are significant compared to navigation system errors an optimal filter is required. The extended Kalman filter is ideally suited for nonlinear estimation problems.

1. Extended Kalman-filter

Kalman-type filter provide the optimal use of all important quantities

- system and measurement dynamics
- assumed statistics of system noises and measurement errors
- initial condition information

to deduce a minimum error estimate. The basic theory developed by R.E. Kalman [6, 7] in 1961 assumes a linear dynamic model, but the algorithm was soon applied to nonlinear guidance and navigation problems in the Apollo program. Such estimation tools attribute the nonlinear system to linear ones by using Taylor series approximation and is called extended Kalman filter [4]. This work is based on the filter equations, which are fully summarized in Table 1. In addition Figure 3 shows the computation scheme by means of an information flow diagram. It presents the main frame of the magnetometer-based autonomous navigation. The quantities appearing in Table 1 are described in the following two sections.

2. Modeling

The applicability of the Kalman filtering technique rests on the availability of an accurate dynamical model as well as the partial derivatives of these models with respect to the state vector. For several reasons it was convenient to use cartesian coordinates for state representation in an inertial reference-axis system. Therefore the six-dimensional state vector consists of spacecraft position and velocity:

$$\underline{x}(t) = (x, y, z, \dot{x}, \dot{y}, \dot{z})^T$$

Table 1: Continuous-Discrete Extended Kalman Filter

System Model Measurement Model Assumptions	$\dot{\underline{x}}(t) = \underline{f}(\underline{x}(t), t) + \underline{w}(t)$ $\underline{z}_k = \underline{h}_k(\underline{x}(t_k)) + \underline{v}_k, \quad k = 1, 2, \ldots$ $\underline{w}(t) \sim N(\underline{0}, \underline{Q}(t)), \underline{v}_k \sim N(\underline{0}, \underline{R}_k), E[\underline{w}(t), \underline{v}_k^T] = 0$
Initial Conditions	$\underline{x}(0) \sim N(\hat{\underline{x}}_0, \underline{P}_0)$
State Estimate Propagation Error Covariance Propagation	$\dot{\hat{\underline{x}}}(t) = \underline{f}(\hat{\underline{x}}(t), t)$ $\dot{\underline{P}}(t) = \underline{F}(\hat{x}(t), t)\underline{P}(t) + \underline{P}(t)\underline{F}^T(\hat{x}(t), t) + \underline{Q}(t)$
State Estimate Update Error Covariance Update Gain Matrix	$\hat{\underline{x}}_k(+) = \hat{\underline{x}}_k(-) + \underline{K}_k [\underline{z}_k - \underline{h}_k(\hat{\underline{x}}_k(-))]$ $\underline{P}_k(+) = \left[\underline{I} - \underline{K}_K \underline{H}_k(\hat{\underline{x}}_k(-))\right] \underline{P}_K(-)$ $\underline{K}_k = \underline{P}_K(-)\underline{H}_k^T(\hat{\underline{x}}_k(-)) \cdot \left[\underline{H}_k(\hat{\underline{x}}_k(-))\underline{P}_K(-)\underline{H}_k^T(\hat{\underline{x}}_k(-)) + \underline{R}_k\right]^{-1}$
Definitions	$\underline{H}_k(\hat{\underline{x}}(-)) \equiv \left.\frac{\partial \underline{h}_k(\underline{x})}{\partial \underline{x}}\right\|_{\underline{x}=\hat{\underline{x}}_k(-)}$ $\underline{F}(\hat{\underline{x}}(t), t) \equiv \left.\frac{\partial \underline{f}(\underline{x}(t), t)}{\partial \underline{x}(t)}\right\|_{\underline{x}(t)=\hat{\underline{x}}(t)}$

For state propagation

$$\dot{\hat{\underline{x}}}(t) = \underline{f}(\hat{\underline{x}}(t), t)$$

has to be solved, where the right-hand side represents the disturbance accelerations. To deduce the best estimate of the spacecraft state the propagation will be updated with regard to the magnetometer measurements by utilizing both the measurement model $\underline{h}$ and the assumed statistics of the system noises $\underline{Q}$ and measurements errors $\underline{R}$. Therefore the error covariance propagation will be done as shown in Figure 2, where the error covariance matrix $\underline{P}$ presents the uncertainty of the state estimate. The system noise $\underline{w}$ and the measurement error $\underline{v}$ are considered as unbiased white noise processes.

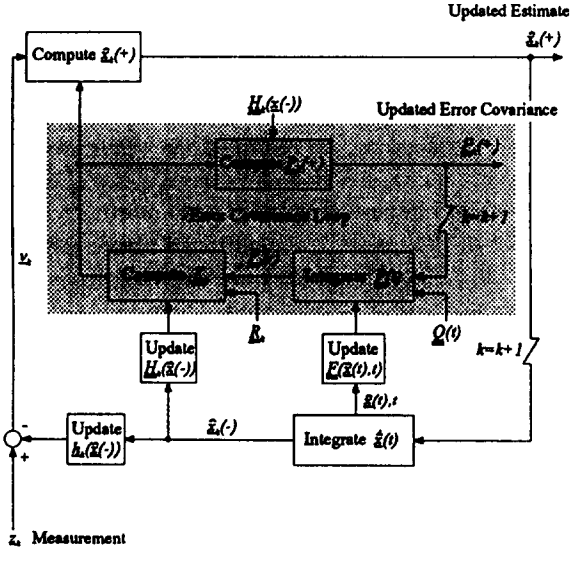

Figure 2: Filter Information Flow Diagram

System Model Newton's laws, a gravitational model with Earth's flattening effects and the modified Harris-Priester atmosphere model [9] are used to propagate the state vector. The error covariance propagation requires the derivatives of the disturbance acceleration with respect to the state vector, which are the components of the system matrix

$$\underline{F} = \left[\begin{array}{c|c} \frac{\partial \underline{v}}{\partial \underline{r}} & \frac{\partial \underline{v}}{\partial \underline{v}} \\ \hline \frac{\partial \underline{a}}{\partial \underline{r}} & \frac{\partial \underline{a}}{\partial \underline{v}} \end{array}\right] = \left[\begin{array}{c|c} \underline{0} & \underline{I} \\ \hline \underline{G} + \underline{D} & \underline{D}_v \end{array}\right] \tag{1}$$

where $\underline{G}$ is derivative of the gravitational disturbance acceleration with respect to the position and $\underline{D}_{,v}$ is derivative of the aerodynamical disturbance acceleration with respect to position and velocity.

Oberservation Model A 10th-order spherical harmonic model of the Earth's magnetic field is used during the updates of the

state vector. The field can be expressed as the gradient of a scalar potential function

$$\underline{B} = -\nabla V$$

V can be conveniently represented by a series of spherical harmonics

$$V(r,\theta,\phi) = a\sum_{n=1}^{k}\left(\frac{a}{r}\right)^{n+1}$$

$$\sum_{m=0}^{n}(g_n^m\cos m\phi + h_n^m\sin m\phi)P_n^m(\cos\theta)$$

where a is the equatorial radius of the Earth; the coefficients g_n^m and h_n^m are those of the IGRF 1985 model [1] with propagation of the secular effects out to the eighth-order; and r, Θ and Φ are the geocentric distance, coelevation and east longitude from Greenwich. The model has been rewritten in cartesian coordinates due to the derivatives with respect to the cartesian state vector.

$$B_x = -\frac{\partial V}{\partial y} =$$

$$\frac{1}{2}\sum_{n=1}^{k}\left(\frac{a}{r}\right)^{n+2}\sum_{m=0}^{n}[(n-m+1)(n-m+2)$$
$$P^{n+1,m-1}(-g^{n,m}\cos(m-1)\phi - h^{n,m}\sin(m-1)\phi)$$
$$+P^{n+1,m+1}(g^{n,m}\cos(m+1)\phi + h^{n,m}\sin(m+1)\phi)]$$

$$B_y = -\frac{\partial V}{\partial x} =$$

$$\frac{1}{2}\sum_{n=1}^{k}\left(\frac{a}{r}\right)^{n+2}\sum_{m=0}^{n}[(n-m+1)(n-m+2)$$
$$P^{n+1,m-1}(g^{n,m}\cos(m-1)\phi - h^{n,m}\sin(m-1)\phi)$$
$$+P^{n+1,m+1}(g^{n,m}\cos(m+1)\phi - h^{n,m}\sin(m+1)\phi)]$$

$$B_z = -\frac{\partial V}{\partial z} =$$

$$\sum_{n=1}^{k}\left(\frac{a}{r}\right)^{n+2}\sum_{m=0}^{n}(n-m+1)$$
$$P^{n+1,m}(g^{n,m}\cos m\phi + h^{n,m}\sin m\phi)$$

$P^{n,m}$ is the Schmidt normalized form of the Gauss functions. The Gaussian coefficients are also Schmidt transformed. Figure 3 shows the total magnetic field intensity at an altitude of 350 km computed by the equations mentioned above.

The derivatives with respect to the state vector has been determined analytically. Therefore, the Hessian matrix $\partial^2 V/\partial\underline{x}$ has to be constituted.

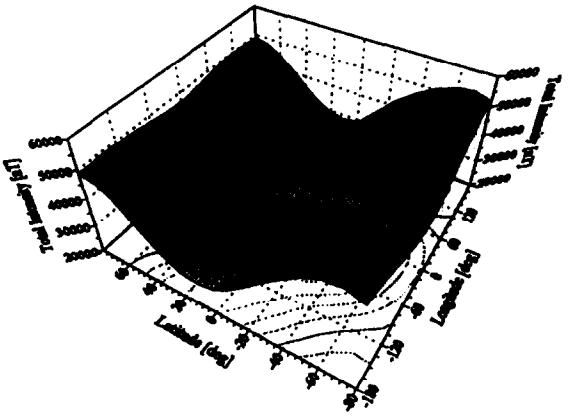

Figure 3: Total Magnetic Field Intensity in nT, epoch 1994, altitude 350 km, 10th-order IGRF model

$$\underline{\underline{J}} = \frac{\partial^2 V}{\partial\underline{x}^2} := \begin{pmatrix} \frac{\partial^2 V}{\partial x^2} & \frac{\partial^2 V}{\partial x\partial y} & \frac{\partial^2 V}{\partial x\partial z} \\ \frac{\partial^2 V}{\partial y\partial x} & \frac{\partial^2 V}{\partial y^2} & \frac{\partial^2 V}{\partial y\partial z} \\ \frac{\partial^2 V}{\partial z\partial x} & \frac{\partial^2 V}{\partial z\partial y} & \frac{\partial^2 V}{\partial z^2} \end{pmatrix}$$

Due to $\underline{\underline{J}}$ is symmetric there is no need to evaluate every matrix element in detail.

$$\frac{\partial^2 V}{\partial x\partial y} = \frac{\partial^2 V}{\partial y\partial x},\ \frac{\partial^2 V}{\partial x\partial z} = \frac{\partial^2 V}{\partial z\partial x},\ \frac{\partial^2 V}{\partial y\partial z} = \frac{\partial^2 V}{\partial z\partial y}$$

Furthermore the magnetic field $\underline{B}$ has zero curl, which means the trace of $\underline{\underline{J}}$ is zero.

$$\frac{\partial^2 V}{\partial x^2} + \frac{\partial^2 V}{\partial y^2} + \frac{\partial^2 V}{\partial z^2} = 0$$

Thus, the required number of second order derivatives decreases from nine to five. The evaluation of these can be obtained via recursive application of the first order derivatives. The necessary differentiations are too numerous to report in this paper. As mentioned above the described algorithm takes only the magnitude of the field vector into account. Consequently, the observable is a scalar quantity.

$$h = \sqrt{B_x^2 + B_y^2 + B_z^2}$$

For that reason the observation matrix $\underline{\underline{H}}$ reduces to a 1×6 vector, where the third to sixth element is zero due to the geomagnetic field is independent of S/C velocity $\underline{v}$. The following formula gives the first three elements, which

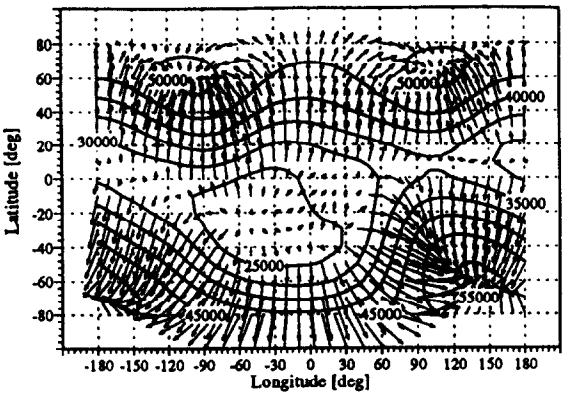

Figure 4: Local Gradient of the Earth's Magnetic Field, altitude 350 km, epoch 1994

are the partial derivatives of h with respect to the S/C position vector $\underline{r}$.

$$\underline{H} = \frac{\partial h}{\partial \underline{r}} = \frac{1}{h} \underline{\underline{J}}\, \underline{B}$$

Figure 4 shows a vector plot of the derivative computation regarding the field of Figure 3. The model of random measurement error statistics has been approximated based on the typical IGRF model accuracy [13].

$$\Delta B_{RMS} = 240 \cdot \left(\frac{a}{r}\right)^3 \; [nT]$$

The system's model of random disturbance statistics has been sized based on the Harris-Priester atmosphere model accuracy, changes in the ballistic coefficient due to the unknown S/C attitude and the neglected higher terms of the gravitational model.

Filter Tuning Filter tuning means the convenient selection of $\underline{\underline{Q}}$, R and $\underline{\underline{P}}^-(t_0)$ to achieve timely convergence to a maximum steady state accuracy. The initial value of the error covariance matrix determines considerably the rapidity of the filter convergence, but has no effect on the steady state filter performance. However $\underline{\underline{Q}}$ and R have influence on transient behavior as well as steady state stability and accuracy. A large system noise covariance matrix $\underline{\underline{Q}}$ compared to the measurement error covariance R yields to rapidity convergence. In this case the valence of measurements is stronger than system behavior. Thus a poorer steady state accuracy will be expected because the filter is over sensitive to poor measurements. If the selection of $\underline{\underline{Q}}$ is too small divergence will occur. Therefore filter tuning is very important to achieve the best estimate of the S/C state.

IV. Filter performance

The first step to examine the filter performance is simulation testing. During this study various simulation tests have been done. Each test consists of four parts:

- Reference state and measurement calculation
- Adding noise to the measurements based on the assumed statistics
- Kalman filtering of the noisy measurements to obtain the best estimate
- Evaluation of results by comparison of best estimate and reference state

For reference state calculation the environment models have been replaced by the sophisticated MSIS90 atmosphere model [5] and an gravitational model, which accounts effects up to $J6$ [9]. The Kalman filter has been tried with a variety of initial errors, several measurement sample rates, diverse shapes of orbits, various initial values for $\underline{\underline{P}}^-(t_0)$ and different process and measurement noise. The BREM-SAT type orbit was of principal interest during the entire study because the satellite was in orbit and operated by ZARM while this work was done. Thus necessary flight data could be obtained easily for performance tests under realistic conditions. The Results will be described in the following section, but first the theoretical filter performance will be considered. Figure 5

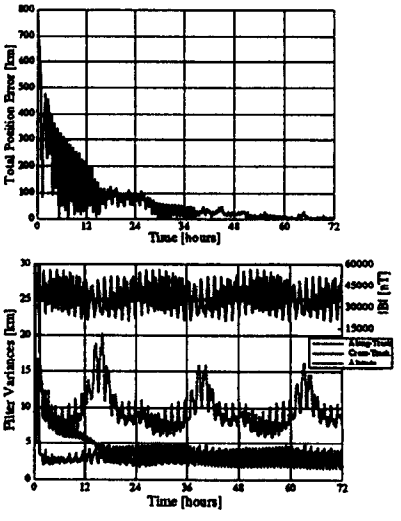

Figure 5: Total Position Error vs Time, Corresponding Filter Variances and Total Geomagnetic Field Intensity for a BREM-SAT Type Orbit; Sample Interval 30 s; v. Type 1/Table 2

shows the total position error history, the corresponding filter variances and the total geomagnetic field intensity.

Figure 5 and 6 are based on the orbital elements, initial values and initial errors are shown in type 1 of Table 2. The achieved root-mean-square error determined over the last 12 hours is 7 km. This convergence indicates observability of the orbit from the total geomagnetic field intensity alone. In steady state along-track, cross-track and altitude errors correspond to the filter variances, so the plots are not shown in this paper. This means also the filter tuning was successful. Most of the errors are in the orbital plane based on the uncertainties of the system model. Especially, the true anomalie or, if the orbit is circular, the sum of true anomalie and the argument of the perigee is difficult to examine. The orbital plane itself is more stiff to the aerodynamic disturbance forces, which are difficult to model. Therefore the inclination i and the right ascension of the ascending node Ω are determined precise by the filter as shown in Figure 6. The plot in Figure 5 also shows the depence of the position of the orbital plane regarding the geomagnetic field, which rotates with respect to the inertial space once per day.

Table 2: Simulation test results; simulation time 72 hours; measurement frequency 30 Hz; measurement error reduced to IGRF model accuracy

type		2	3	4	5	6
a	$[km]$	6699.4	7000	7170	6699	6785
ϵ	$[-]$	0.00134	0.05	0.001	0.00134	0.0125
i	$[grad]$	56.96	57	97	5	97
ω	$[grad]$	160	0	160	160	160
Ω	$[grad]$	317.25	210	317	317.25	317
φ	$[grad]$	287.9	90	287	287.9	287
initial values and errors						
Δa	$[km]$	100	10	10	10	15
$\Delta\epsilon$	$[-]$	0.0007	0.005	0.0005	0.0003	0.0025
Δi	$[grad]$	4	1	1	1	1
$\Delta\omega$	$[grad]$	0	0	0	0	0
$\Delta\Omega$	$[grad]$	4	2	3	3	3
$\Delta\varphi$	$[grad]$	5	2	2	4	2
Δr	$[km]$	866	739.8	234.0	823.7	222
Δv	$[m/s]$	56.8	22.8	59.6	39.8	1
$\sigma_{Q_{x,y,z}}$	10^{-5}	$5 \cdot 10^{-7}$	$2 \cdot 10^{-5}$	10^{-6}	10^{-5}	10^{-6}
σ_R	$[nT]$	200	185	170	200	195
achieved steady state accuracy						
$\Delta r^{\dagger\dagger}$	$[km]$	7	14	3	19	2

†† rms-error determinded over the last 12 hours;

For that reason the observability varies on a daily basis. The main peaks in the along-track variance based on the main field's dipole axis canted with respect to the North

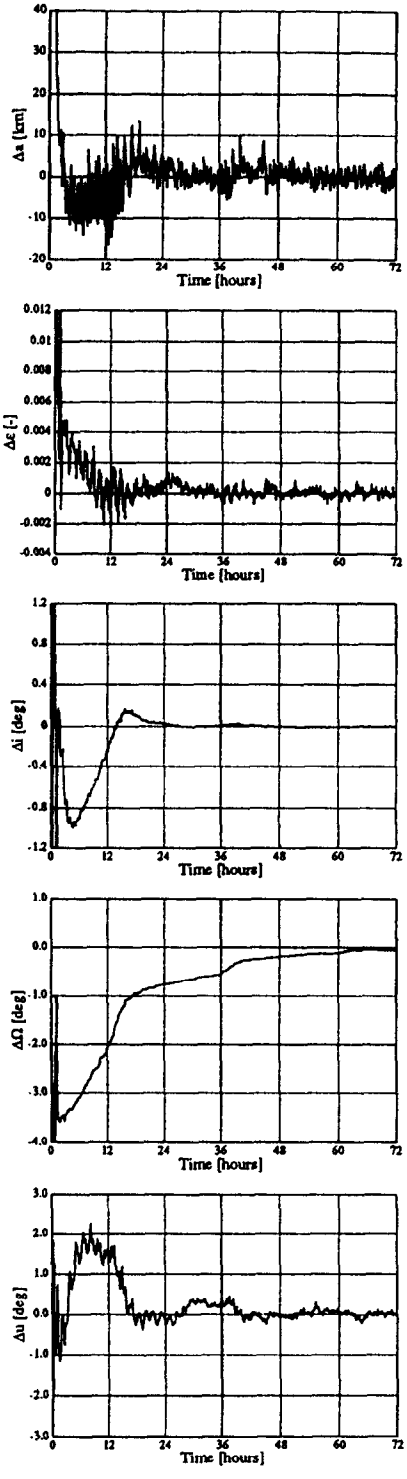

Figure 6: Errors in Keplerian Elements for a BREM-SAT Type Orbit; Sample Interval 30 s; v. Type 1/Table 2

Pole. However, the achieved accuracy is encouraging. Table 2 presents some additional test results of different kinds of orbits. In short words the filter performance decreases with the inclination due to larger partial field derivatives and increases slowly with altitude and eccentricity.

V. BREM-SAT performance

The 63 kg light-weight BREM-SAT was designed and built by ZARM in cooperation with several institutes and companies. The scientific university satellite was of an cylindrical shape with a diameter of 480 mm and a height of 520 mm. BREM-SAT was dedicated to six scientific experiments. The satellite was launched by the Space Shuttle in February 1994. After one year successfully operated by ZARM, the satellite heats up in the atmosphere as expected according to the initial altitude of almost 350 km. Because of technical problems with the starsensor magnetometer measurements became important to determine the actual attitude by using a rough geometrical algorithm [8]. However, the low preciseness was sufficient to fulfill mission requirements. At that time it was decided to develop an autonomous position and attitude system based on magnetometer measurements. This paper presents the first part of these work. The second part, the attitude determination and control system, is under construction but will be finished in near future.

1. Magnetometer calibration

Originally, the magnetometer had been only used to determine the Earth's magnetic field polarity. Thus, it was a low precise, inaccurate calibrated sensor. Therefore, a bias and sensitivity determination procedure has been developed which is independent of the attitude. The used batch estimator utilizing a long segment of magnetometer data, the corresponding position data and the IGRF model to deduce the best estimate of bias and sensitivity for the three axis. For the ith point, the field magnitude error $\delta_i(\underline{b}, \underline{e})$ is defined by

$$\delta_i(\underline{b}, \underline{e}) = |\underline{B}_{c_i}|^2 - |\underline{e}\,\underline{\underline{M}}_i - \underline{b}|^2$$

if a linear characteristic is assumed. The quantities are:

- $\underline{B}_{c_i}$ = magnetic field model intensity at time i
- $\underline{\underline{M}}_i$ = magnetometer reading at time i (3×3 diagonal matrix)
- $\underline{b}$ = bias-vector
- $\underline{e}$ = sensitivity-vector

The optimal values of $\underline{b}$ and $\underline{e}$ are that which minimize the loss functions

$$L(\underline{b}) = \frac{1}{2}\sum_{i=1}^{N} |\delta_i(\underline{b}, \underline{e})|^2$$

where N is the number of measurements. Thus, the first-order derivative with respect to $\underline{b}$ and $\underline{e}$ have to be zero. The details of the necessary differentiations are to numerous to report here. The developed determination equations are solved iteratively with the Newton-Raphson method, i.e. the second-order derivative is also needed.

$$(\hat{\underline{e}}, \hat{\underline{b}})_{k+1} = (\hat{\underline{e}}, \hat{\underline{b}})_k - \left(\frac{\partial L(\hat{\underline{e}}, \hat{\underline{b}})_k}{\partial(\hat{\underline{e}}, \hat{\underline{b}})_k}\right)\left(\frac{\partial^2 L(\hat{\underline{e}}, \hat{\underline{b}})_k}{\partial(\hat{\underline{e}}, \hat{\underline{b}})_k^2}\right)^{-1}$$

Figure 7 shows the achieved accuracy compared with the IGRF model.

2. Results with BREM-SAT data

Magnetometer data from the BREM-SAT mission have been used to evaluate the developed navigation scheme under real conditions. Because of the low preciseness of the used sensor, the achieved estimate accuracy is comparable low but correspond to simulation tests done with the same assumed statistics. The BREM-SAT tests involves filtering of the

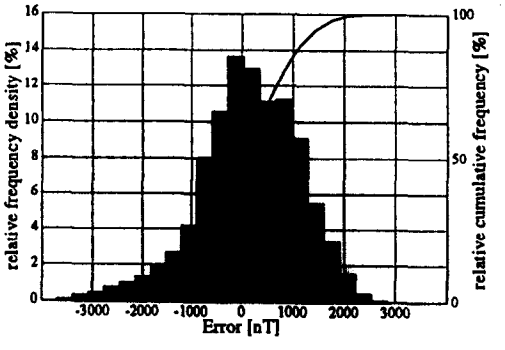

Figure 7: Difference between Magnetometer Readings and IGRF Model; RMS-Error 985 [nT]; Bias 135 [nT]; 1000 Measurements, sample rate 300 s

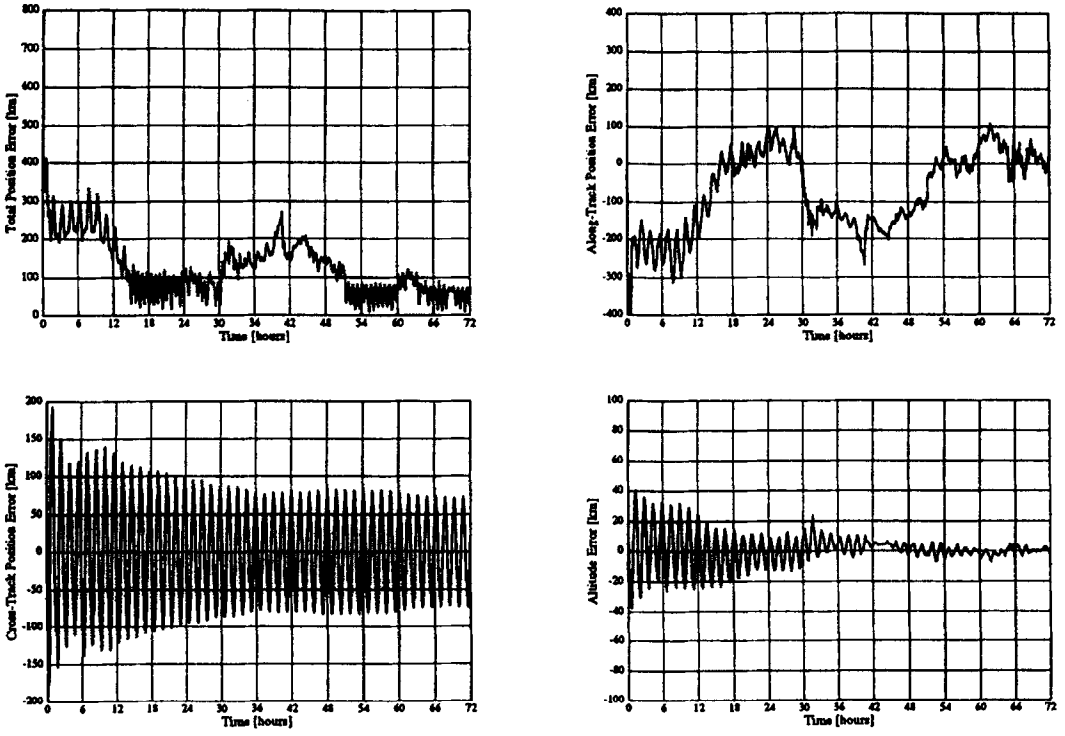

Figure 8: Results with BREM-SAT Flight Data; Sample Rate 300 s;

calibrated magnetometer readings followed by comparison of the results with position derived from the one-way Doppler frequency shift [2] or NASA's Two Line Elements.

Figure 8 shows the typical filter result for a three days magnetometer data sequence. The periodic cross-track error implies some inaccuracy of determination of the orbital plane. Especially, the longitude of the ascending node cannot be determined precise. However, the altitude error is comparable low. The total position rms-error of the last 24 hours is 70 km. In each test case the filter is stable and converges, even though the accuracy is rather low. That means the orbit is observable from magnetometer measurements alone, even if the sensor is very inaccurate.

VI. Conclusion

It has been shown that low Earth's orbits are fully observable from the total intensity of the Earth's magnetic field. Therefore, the developed fully autonomous low cost navigation scheme is independent of S/C attitude. Total position root-mean-square error of less than 10 km can be achieved if a precise magnetometer is used. Thus, the system provides sufficient accuracy for most missions and requires solely a three-axis magnetometer and computation time on the on-board computer. Moreover it can be used as a backup system to provide both redundancy and low system expense. Furthermore, this work can be seen as the first part of a fully autonomous magnetometer-based position and attitude determination and control system. The attitude determination system will be finished in the near future and will be used for post mission attitude determination of the BREM-SAT mission needed for experiment data analyzation. Besides the algorithm is proposed to the small astronomical satellite ABRIXAS for low precise pointing operations and as a backup system. The necessary position data will be provided by a GPS system or, if full autonomy is required, by the magnetometer-based system itself.

Acknowledgments

I wish to thank Prof. Rath from the Center of Applied Space Technology and Microgravity for making this study possible and Prof. Rex from the Institute of Space Flight Technology and Nuclear Reactor Technology for supporting this work. I like to thank H. Königsmann

and the BREM-SAT team for several crucial and helpfull hints. I also like to thank B. Schlarmann for supplying me with the processed position data.

References

[1] BARRACLOUGH, D.R., (Chairman IAGA Division Working Group 1), "International Geomagnetic Reference Field Revision 1987", J. Geomag. Geoelectr., 39, 773-779, 1987

[2] SCHLARMANN, B.KL., "Orbit Determination During the BREM-SAT Mission," *45th Congress of the International Astronautics Federation*, IAA-94-IAA.11.3.769, Jerusalem, Israel, October 9-14, 1994

[3] FOX, S.M., PAL, P.K., PSIAKI, M.L., "Magnetometer-Based Autonomous Satellite Navigation (MAGNAV)," *Guidance and Control 1990; Proceedings of the Annual Rocky Mountain Guidance and Control Conference* (Keystone, CO), American Astronautical Society, San Diego, CA, 1990, pp. 369-382, (AAS Paper 90-051).

[4] GELB, A. (Ed.), *Applied Optimal Estimation*, The M.I.T. Press, Cambridge, Massachusetts, 1974

[5] HEDIN, ALAN E., "Extension of the MSIS Thermosphere Model into the Middle and Lower Atmosphere", *Journal of Geophysical Research*, Vol. 96, 1991, No. A2, Pages 1159-1172.

[6] KALMAN, R.E., "A New Approach to Linear Filtering and Prediction Problems", *Journal of Basic Engineering (ASME)*, Vol. 82D, No. 1, March 1960, pp.35-45.

[7] KALMAN, R.E., BUCY, R.S., "New Results in Linear Filtering and Prediction Theory", *Journal of Basic Engineering (ASME)*, Vol. 83D, No. 1, March 1961, pp.95-107.

[8] KÖNIGSMANN, H.J., OELZE, H.W., RATH, H.J., "BREM-SAT - First Flight Results," *Proceedings of the 8th Annual AIAA/USU Conference on Small Satellites*, Utah State University, Logan, UT, 1994

[9] LONG, A.C., CAPPELLARI, J.O., VELEZ, C.E., FUCHS, A.J., "Goddard Trajectory Determination System (GTDS) Mathematical Theory (Revision1)", Goddard Space Flight Center, Greenbelt, Maryland, Computer Science Corporation, Lanham-Seabrook, Maryland, FDD/552-89/0001 and CSC/TR-89/6001, July 1989

[10] PSIAKI, M.L., MARTEL, F., "Autonomous Magnetic Navigation for Earth Orbiting Spacecraft," *Proceedings of the 3rd Annual AIAA/USU Conference on Small Satellites*, Utah State University, Logan, UT, 1989

[11] PSIAKI, M.L., LEJIN H., FOX, S.F., "Ground Tests of Magnetometer-Based Autonomous Navigation (MAGNAV) for Low-Earth-Orbiting Spacecraft," *Journal of Guidance, Control and Dynamics*, Vol. 16, No. 1, January-February 1993, pp.206-214.

[12] SOMMER, WIDJAJA, WILDE, "Study of Onboard Orbit Determination (OBOD)", ESA Contract Number : 7463/87/D/IM(SC), Bremen, 1989

[13] WERTZ, JAMES R. (Ed.), *Spacecraft Attitude Determination and Control*, D. Reidel Publishing Company, Boston, U.S.A., 1978

[14] WIEGAND, M., "Autonome Satelliten-Navigation mittels Kalman-Filterung von Magnetometerdaten am Beispiel des Kleinsatelliten BREM-SAT", Studienarbeit R-9501, IfRR TU Braunschweig, Januar 1995